NASA TECHNICAL TRANSLATION NASA TT F-15,713

ON THE USE OF BRANCH MODES FOR THE CALCULATION OF HELICOPTER STRUCTURAL DYNAMIC CHARACTERISTICS

C. T. Tran, W. Twomey, and R. Dat

Translation of "Calcul des caractéristiques dynamiques d'une structure d'hélicoptère par la méthode des modes partiels," La Recherche Aérospatiale, No. 6 (November -December), 1973, pp. 337-354

(NASA-TT-P-15713) ON THE USE OF BRANCH MODES FOR THE CALCULATION OF HELICOPTER STRUCTURAL DYNAMIC CHARACTERISTICS (Kanner (Leo) Associates) 45 p HC $5.25

N74-27503

CSCL 01C G3/02

Unclas 43161

NATIONAL AERONAUTICS AND SPACE ADMINISTRATION
WASHINGTON, D.C. 20546 JULY 1974

ON THE USE OF BRANCH MODES FOR THE CALCULATION OF HELICOPTER STRUCTURAL DYNAMIC CHARACTERISTICS

C.T. Tran, W. Twomey, and R. Dat
National Office of Aerospace Study and Research

Introduction

It is much more difficult to predict and analyze aeroelastic /338* phenomena for helicopters than it is for fixed-wing aircraft, since in the former case these phenomena assume much more complex and varied forms. In addition to instability factors which may be manifested by divergent natural vibrations and which produce aircraft flutter, in forward flight there are al o forced vibrations attendant on periodic variations in the aerodynamic field around the blades.

For several years, the O.N.E.R.A. [National Office of Aerospace Study and Research], in collaboration with designers, has been involved in the development of methods of calculation which would make it possible to predict these phenomena.

As in the case of aircraft, analysis of the aeroelasticity of helicopters draws on two disciplines:

-- non-stationary aerodynamics, which makes it possible to predict the aerodynamic forces acting on the blades when their movement characteristics are given,

-- structural dynamics, making it possible to predict the response of the blades and the fuselage when the forces applied to the blades are known.

The non-stationary aerodynamics of helicopters has already been treated in references [1], [2] and [3].

---

*Numbers in the margin indicate pagination in the foreign text.

This article will be concerned with calculation of structural characteristics. Theoretical and experimental results will be compared after a review of the computational procedure used.

On the basis of the experience gained with aircraft, a few years ago the O.N.E.R.A. proposed to apply the modal representation to helicopters [4]. In this case, however, it was natural to break down the structure into several parts (the fuselage and rotor hub on the one hand, and the blades on the other) and to define each of these components by its appropriate modes. The structure is thus said to be represented by "branch modes."

The calculations make it possible to reconstruct the complete structure with rotating blades by introducing the linkage conditions and the inertial forces of coupling and rotation.

The application of Lagrange equations and linearization, which is justified to the extent that the vibrations are assumed to be of low amplitude, results in a system of linear differential equations generally including a given number of periodic coefficients.

This method is described in Refs. [4] and [5].

The formulation given in Ref. [4] is adapted to the study of forced periodic vibration. In this case, expansion into a Fourier series makes it possible to determine the responses without the encumbrance of periodic coefficients.

However, in order to be able to deal with the problems of characteristic movement in addition, it is preferable to eliminate periodic coefficients by choosing a system of coordinates making use of the symmetry of the rotor. Here, differential equations with constant coefficients are obtained.

The solutions for the system of equations without a second member define natural vibration modes for the fuselage-rotor assembly.

The purpose of the present article is to show the validity of the branch mode method by comparison with the results of measurements performed on a schematic helicopter model. Considering that the natural vibration modes of the fuselage-rotor assembly define its dynamic characteristics, the comparison makes use of these modes, which are both measured and computed.

This control complements the check described in Ref. [4] dealing with an actual helicopter with rotor at rest.

Theoretical Formulation

The equations governing the vibrational behavior of a structural unit consisting of a three-blade rotor mounted atop a fuselage will be described, taking into account deformation of the blades and the fuselage.

The fuselage is activated with low-amplitude movements around its equilibrium position.

The rotor is activated with rotation at a finite speed, Θ, and small movements which include:

- oscillations around the polar axis, or hub,
- drive oscillations due to the rotary head which is connected to the fusilage,
- vibrations due to deflection of the blades.

The theoretical formulation given in ref. [5] will be reviewed briefly in this section. After expressions for kinetic energy, potential energy, and the dissipation function of the fuselage and

the blades haye been given, the Lagrange equations governing the behavior of the entire s:ructure will be constructed.

1. Movement of a Blade Component

Defined below are several orthonormal bases which make it possible conveniently to introduce the effect of rotation and to express the speed of various points on the blades.

$S(\vec{i}, \vec{j}, \vec{k})$ is an absolute basis positioned and oriented as indicated by Fig. 1a.

$S_1(\vec{i}_1, \vec{j}_1, \vec{k}_1)$ is obtained by rotating S about i by a small angle $\phi(t)$.

$S_2(\vec{i}_2, \vec{j}_2, \vec{k}_2)$ is obtained by rotating S_1 about j_1 by a small angle $\psi(t)$.

$S_3(\vec{i}_3, \vec{j}_3, \vec{k}_3)$ is obtained by rotating S_2 about k_2 by a finite angle $\theta(t) - \frac{\pi}{2}$.

$\varphi(t), \psi(t)$ denote the roll and pitch oscillations of the rotor head, respectively.

$\theta(t)$ is the azimuth of the blade considered in Fig. 1a, and S_3 is the basis related to it.

Since the rotor consists of three blades separated by a difference in azimuth of $\frac{2\pi}{3}$, the azimuth of each blade will be designated more precisely by $\theta_k(t)$, with K = 1, 2, 3. The blade of reference in Fig. 1 being designated by K = 1, as a result: /339

$$\theta_K(t) = \theta_1(t) + \frac{2\pi}{3}(K-1), \quad K = 1, 2, 3.$$

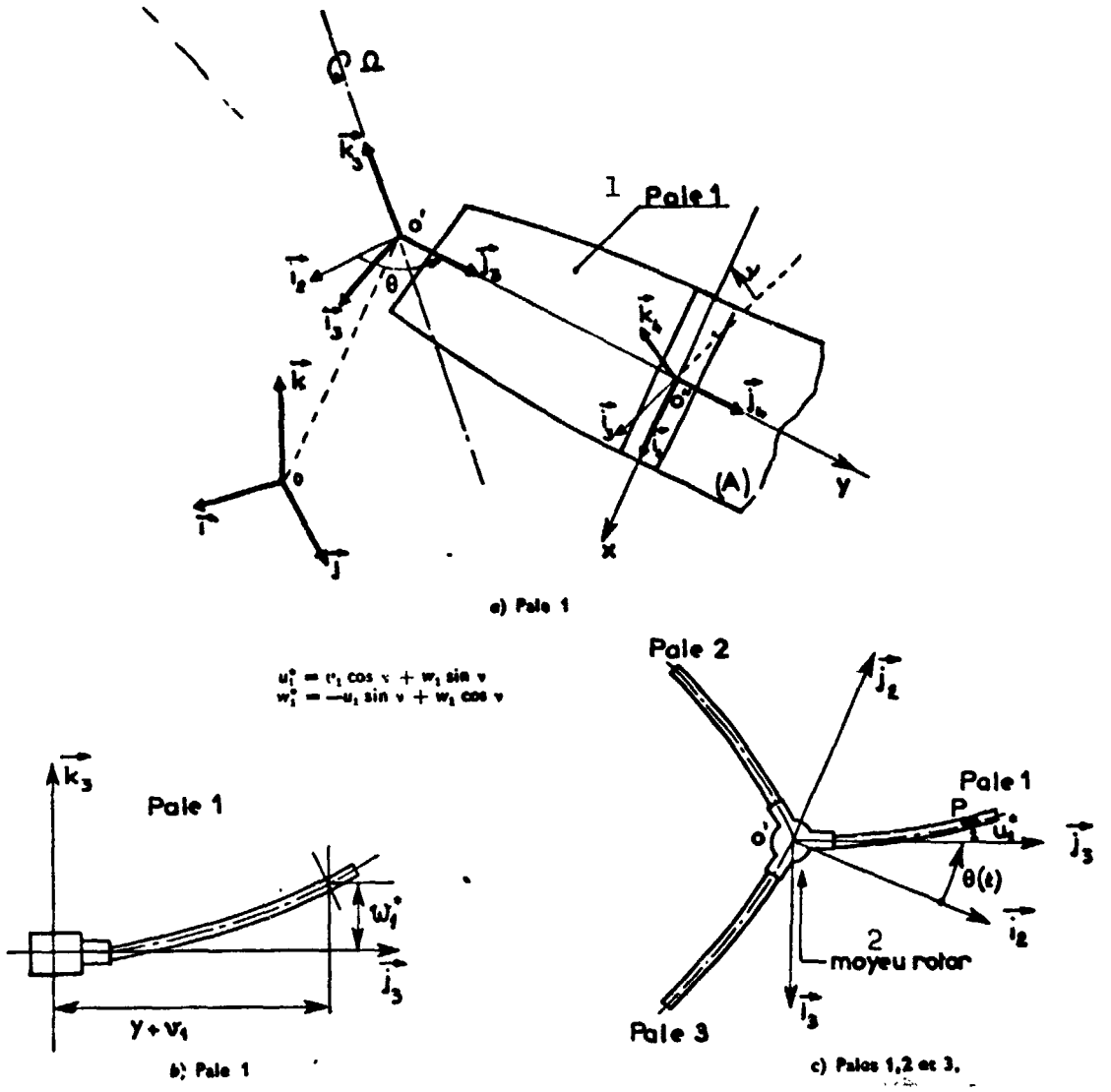

Fig. 1. Rotational movements.

Key: 1. Blade (typ.).
2. Rotor hub.

Given that the movement of the rotor consists of rotation at a finite constant speed, Ω, and low-amplitude oscillation, the result is:

$$\theta_K(t) = \Omega t + \frac{2\pi}{3}(K-1) + \Delta\theta(t),\ K = 1, 2, 3.$$

$\Delta\theta(t)$ defining the consecutive angular difference at low-amplitude azimuthal oscillations of the rotor.

Since the thickness of the blades is slight in comparison to their chord and span, these structures will be defined as regular surfaces with a surface density σ. Spin, which depends on the radial coordinate y, is designated by $\nu(y)$.

To denote the points on a blade, a local basis $S_4(\vec{i}_4, \vec{j}_4, \vec{k}_4)$ is defined by rotating S_3 about j_3 by an angle $\nu(y)$.

In the absence of deformation, a random point on the blade K is denoted by the position vector

$$\vec{R}_K = S_4 \begin{pmatrix} x \\ y \\ 0 \end{pmatrix} \tag{1.1}$$

where x is the chord coordinate and y the span or radial coordinate.

The elastic deformation of the blade is represented by the de- /340
formation vector (fig. 1)

$$\vec{r}_K(t) = S_4 \begin{pmatrix} u_K \\ v_K \\ w_K \end{pmatrix} \tag{1.2}$$

$|\vec{r}_K|$ is an infinitely small first order quantity, w_K is the deflection normal to the blade, u_K the coplanar deflection and v_K a second order longitudinal displacement attendant on the transverse deflections u_K and w_K, whose precise value will be determined later on.

The translational oscillations of the hub, connected to the fuselage, are denoted by the components ξ, η, ζ, within basis S. Corresponding to these factors is the drive speed of the rotor defined by the vector:

$$\vec{V}_0(t) = \dot{\vec{O}}\dot{\vec{O}} = S\begin{pmatrix}\dot{\xi}\\ \dot{\eta}\\ \dot{\zeta}\end{pmatrix} \tag{1.3}$$

where ξ, η, ζ, are infinitely small quantities of the first order.

The resultant rotational speed of the rotor head is given by:

$$\vec{\Omega}_R(t) = S\begin{pmatrix}\dot{\varphi}\\ 0\\ 0\end{pmatrix} + S_1\begin{pmatrix}0\\ \dot{\psi}\\ 0\end{pmatrix} + S_2\begin{pmatrix}0\\ 0\\ \dot{\theta}\end{pmatrix}. \tag{1.4}$$

Bases S, S_1, ... S_4 are interconnected by classical rotation matrices. Thus:

$$S_1 = SK_1,\quad S_2 = S_1K_2,\quad S_3 = S_2K_3,\quad S_4 = S_3K_4$$

with

$$K_1 = \begin{pmatrix}1 & . & .\\ . & \cos\varphi & -\sin\varphi\\ . & \sin\varphi & \cos\varphi\end{pmatrix},\qquad K_2 = \begin{pmatrix}\cos\psi & . & \sin\psi\\ . & 1 & .\\ -\sin\psi & . & \cos\psi\end{pmatrix}$$
$$K_3 = \begin{pmatrix}\sin\theta_K & \cos\theta_K & .\\ -\cos\theta_K & \sin\theta_K & .\\ . & . & 1\end{pmatrix},\qquad K_4 = \begin{pmatrix}\cos\nu & . & \sin\nu\\ . & 1 & .\\ -\sin\nu & . & \cos\nu\end{pmatrix}. \tag{2}$$

These equations make it possible to express the vectors $\vec{R}_K$, $\vec{r}_K$, $\vec{V}_0$, $\vec{\Omega}_R$ within a single basis, for example within S_3.

The absolute speed of a point P on the blade k is given by:

$$\vec{V}_K = \vec{V}_0 + \vec{\Omega}_R \wedge (\vec{R}_K + \vec{r}_K) + \dot{\vec{r}}_K \tag{3}$$

Eqs. (1), (2) and (3) make it possible to express $\vec{V}_i$ within basis S_3. Since the functions denoting small vibrational movements are first order quantities, there is no need to take into account terms of an order greater than 2 which have no influence on the kinetic energy of the system.

As a result:

$$\vec{V_K} = S_3 \begin{pmatrix} -\dot{\varphi}\dot{\psi}y - \dot{\theta}v_K - \dot{\theta}y + \dot{u}_K^\circ \\ \dot{\varphi}\dot{\psi}x\cos\nu + \dot{v}_K + \dot{\theta}x\cos\nu + \dot{\theta}u_K^\circ \\ \dot{w}_K^\circ \end{pmatrix} + S_3 \begin{pmatrix} w_K^\circ\cos\theta_K & w_K^\circ\sin\theta_K \\ -w_K^\circ\sin\theta_K & w_K^\circ\cos\theta_K \\ -u_K^\circ\cos\theta_K & -u_K^\circ\sin\theta_K \end{pmatrix} \begin{pmatrix} \dot{\varphi} \\ \dot{\psi} \end{pmatrix}$$

$$+ S_3 \begin{pmatrix} . & . & -\varphi\cos\theta_K - \psi\sin\theta_K \\ . & . & \varphi\sin\theta_K - \psi\cos\theta_K \\ \psi & -\varphi & \end{pmatrix} \begin{pmatrix} \dot{\xi} \\ \dot{\eta} \\ \dot{\zeta} \end{pmatrix} + S_3 \begin{pmatrix} Z_K\cos\theta_K & Z_K\sin\theta_K & \sin\theta_K & -\cos\theta_K \\ -Z_K\sin\theta_K & Z_K\cos\theta_K & \cos\theta_K & \sin\theta_K \\ Y_K & -X_K & . & . \quad 1 \end{pmatrix} \begin{pmatrix} \dot{\varphi} \\ \dot{\psi} \\ \dot{\xi} \\ \dot{\eta} \\ \dot{\zeta} \end{pmatrix} \qquad (4)$$

with

$$X_K = x\cos\nu\sin\theta_K + y\cos\theta_K, \quad Y_K = -x\cos\nu\cos\theta_K + y\sin\theta_K,$$

$$Z_K = -x\sin\nu, \quad u_K^\circ = u_K\cos\nu + w_K\sin\nu, \quad w_K^\circ = -u_K\sin\nu + w_K\cos\nu.$$

In order to determine the longitudinal displacement V_K of a point P on the blade, it is assumed that the average fiber, which coincides with the axis Oy in the at-rest position, is deformed in the coplanar (u_K) and normal (w_K) direction, its length remaining constant. Deflections u_K and w_K being of the first order, this condition results in a second order longitudinal displacement given by:

$$v_K = -\frac{1}{2}\int_0^y \left[\left(\frac{\partial u_K}{\partial y_0}\right)^2 + \left(\frac{\partial w_K}{\partial y_0}\right)^2\right] dy_0.$$

The existence of this longitudinal deflection will make it possible to introduce the potential work of centrifugal force in calculation of the kinetic energy.

II. 2 Modal Representation. Generalized Coordinates for Fuselage and Blade /341

The modal representation should be applied separately to the fuselage and to each of the blades.

Let $\vec{U}(P,t)$ be the vector field defining the movement of points P of the fuselage. One assumes:

$$\vec{U}(P, t) = \sum_{i=1}^{n} \vec{U}_i(p) q_i(t)$$

where the functions $\overset{*}{U}_i(p)$ are the characteristic vibrational shapes of the fuselage-hub assembly without blades.

The functions $q_i(t)$ are the generalized fuselage coordinates.

Small displacements ofthe rotor head, connected to the fuselage, are also determined by the means of the fuselage coordinates. Thus:

$$\varphi = \sum_i \varphi_i q_i(t), \quad \psi = \sum_i \psi_i q_i(t), \quad \xi = \sum_i \xi_i q_i(t)$$
$$\eta = \sum_i \eta_i q_i(t), \quad \zeta = \sum_i \zeta_i q_i(t)$$

where $\varphi_i, \psi_i, \xi_i, \eta_i, \zeta_i$ are the values for the components of angular displacement and translation of the rotor head in mode i.

Similarly, for each blade K, the normal and coplanar deflections are expressed by:

$$w_K(x, y, t) = \sum_{i=1}^{m} w_i(x, y)\, s_{iK}(t)$$
$$u_K(y, t) = \sum_{i=1}^{m} u_i(y)\, s_{iK}(t)$$

where the coordinate functions $\omega_i(x,y)$ and $u_i(y)$ denote the characteristic vibrational shapes of the blades, assumed to be connected to a fixed hub.

The functions $s_{iK}(t)$ are the generalized blade coordinates.

In each mode i, the deflection $w_i(x,y)$ may be broken down into bending or flapping, and deflection due to torsion, assuming:

$$w_i(x, y) = w_{0i}(y) + x\,\phi_i(y)$$

$w_{\theta i}(y)$ denoting deflection due to flapping in the characteristic shape i of the blade, $\phi_i(y)$ denoting torsion, and $u_i(y)$ denoting deflection due to drag.

The blades will be assumed to be identical, with the result that the functions $u_i(y)$, $\phi_i(y)$ and $w_{\theta i}(y)$, which define the modes of characteristic shape are the same for all three blades.

The coordinates q_i, s_{iK} and the azimuthal variations $\Delta\theta$ completely determine small movements of the rotor-fuselage assembly.

The function q(t) will be used to designate the column of fuselage coordinates and $s_K(t)$ the column of generalized coordinates of a blade K.

II. 3 Kinetic Energy, Potential Energy and Dissipation Function

Eq. (4) makes it possible to estimate the kinetic energy of the blades. Adding the kinetic energy of the fuselage, this equation becomes:

$$2T = \dot{\theta}^2 I_{z_T} + 2\dot{\theta}\sum_K \Lambda \dot{s}_K + 2\dot{\theta}^2 \sum_K \Gamma s_K + 2\dot{\theta}\bar{q} A q - \dot{\theta}^2 \sum_K \bar{s}_K \phi s_K - 2\dot{\theta}\sum_K \bar{s}_K H s_K + \bar{q} M \dot{q} + \sum_K \bar{s}_K \mu \dot{s}_K + 2\sum_K \bar{q}\left[F + \cos\theta_K G + \sin\theta_K J\right]\dot{s}_K + 2\dot{\theta}\sum_K \dot{q}\left[\cos\theta_K \ldots \sin\theta_K T\right] s_K \quad (5.1)$$

where I_{zT} is the polar inertial moment of the rotor assembly, including the engine.

Λ and Γ are lines and A, ϕ H, M, μ, E, G, J, S and T are matrices obtained by integrating over one blade (A) or over the structure excluding the blades (F).

The result is:

$$\Lambda_i = -\iint_{(A)} y\,(u_i \cos\nu + w_i \sin\nu)\,\sigma\,dx\,dy$$

$$\Gamma_i = \iint_{(A)} x\cos\nu\,[\,u_i \cos\nu + w_i \sin\nu]\,\sigma\,dx\,dy$$

$$A_{ij} = I_z \varphi_i \psi_j$$

$$\phi_{ij} = \iint_{(A)} y \int_0^y \left(\frac{\partial u_i}{\partial y_0}\frac{\partial u_j}{\partial y_0} + \frac{\partial w_i}{\partial y_0}\frac{\partial w_j}{\partial y_0}\right) dy_0\,\sigma\,dx\,dy - \iint_{(A)} \left[u_i u_j \cos^2\nu + (u_i w_j + u_j w_i)\sin\nu\cos\nu + w_i w_j \sin^2\nu\right]\sigma\,dx\,dy$$

$$H_{ij} = \iint_{(A)} x\cos\nu \int_0^y \left(\frac{\partial u_i}{\partial y_0}\frac{\partial u_j}{\partial y_0} + \frac{\partial w_i}{\partial y_0}\frac{\partial w_j}{\partial y_c}\right) dy_0\,\sigma\,dx\,dy$$

$$\mu_{ij} = \iint_{(A)} (u_i u_j + w_i w_j)\,\sigma\,dx\,dy$$

/342

$$M_{ij} = I_{pz}\left[\varphi_i\varphi_j + \psi_i\psi_j\right] + S_{pz}\left[\psi_i\xi_j + \xi_i\psi_j - \varphi_i\tau_j - \eta_i\varphi_j\right] + M_p\left[\xi_i\xi_j + \eta_i\eta_j + \zeta_i\zeta_j\right] + \iiint_{(P)} \rho(p)\,\vec{U}_i(p)\,\vec{U}_j(p)\,d\Omega$$

$$F_{ij} = \zeta_i \iint_{(A)} (-u_j \sin\nu + w_j \cos\nu)\,\sigma\,dx\,dy$$

$$G_{ij} = -\varphi_i \iint_{(A)} x\,w_j\,\sigma\,dx\,dy + \psi_i \iint_{(A)} y\,(u_j \sin\nu - w_j \cos\nu)\,\sigma\,dx\,dy - \tau_i \iint_{(A)} (u_j \cos\nu + w_j \sin\nu)\,\sigma$$

$$J_{ij} = -\varphi_i \iint_{(A)} y\,(u_j \sin\nu - w_j \cos\nu)\,\sigma\,dx\,dy - \psi_i \iint_{(A)} x\,w_j\,\sigma\,dx\,dy + \xi_i \iint_{(A)} (u_j \cos\nu + w_j \sin\nu)\,\sigma\,dx\,dy$$

$$S_{ij} = \varphi_i \iint_{(A)} y\,(u_j \sin\nu - w_j \cos\nu)\,\sigma\,dx\,dy + \psi_i \iint_{(A)} x\,(w_j(\cos^2\nu - \sin^2\nu) - 2u_j \sin\nu\cos\nu)\,\sigma\,dx\,dy + \xi_i \iint_{(A)} (u_j \cos\nu + w_j \sin\nu)\,\sigma\,dx\,dy$$

$$T_{ij} = -\varphi_i \iint_{(A)} x\,(w_j(\cos^2\nu - \sin^2\nu) - 2u_j \sin\nu\cos\nu)\,\sigma\,dx\,dy + \psi_i \iint_{(A)} y\,(u_j \sin\nu - w_j \cos\nu)\,\sigma\,dx\,dy + \tau_i \iint_{(A)} (u_j \cos\nu + w_j \sin\nu)\,\sigma\,dx\,dy.$$

The moment of polar inertia I_z applies to a structure consisting of the blades and the part of the rotor integral with the hub.

I_{px}, S_{px} and I_p pertain to the blade assembly and respectively designate the inertial moment in relation to Ox_2 (or Oy_2) the static moment in relation to the plane of the rotor $\left(\int z_3\, dm\right)$ and the weight.

μ is the generalized blade weight matrix.

Similarly, the integral $\iiint_{(\sigma)} \rho \vec{U}_i \vec{U}_j\, d\Omega$ denotes the generalized weight μ^*_{ij} of the helicopter excluding the blades. It will be noted that the functions are orthogonal:

$$\mu_{ij} = 0 \text{ et } \mu^*_{ij} = 0 \text{ for } i \neq j.$$

In addition, the matrices M, ϕ, and H are Hermitian.

The potential energy U of the system may be written:

$$2U = \bar{q}\gamma^* q + \sum_K \bar{e}_K \gamma e_K \tag{5.2}$$

Similarly, for the dissipation function:

$$2D = \bar{\dot{q}}\beta^* \dot{q} + \sum_K \bar{\dot{e}}_K \beta \dot{e}_K \tag{5.3}$$

where γ^* and β^* respe tively denote generalized rigidity and damping matrices for the helicopter exclusive of the blades.

γ and β respectively denote the generalized rigidity matrix and generalized damping matrix for a single blade.

On the bases of characteristic shape, matrices γ^* and γ are diagonal.

On the basis of Eqs. (5.1), (5.2) and (5.3) it is possible to construct the Lagrange equations for the generalized coordinates q, s_K, and $\Delta\theta$.

These equations form a second order linear differential system containing periodic coefficients resulting from the presence of sin θ_K and cos θ_K terms in the equation for kinetic energy (5.1).

II. 4 Generalized Rotor Coordinates

In an analysis of the periodic vibrations produced in a helicopter moving forward at constant speed, the difficulty due to the periodic coefficients may be overcome by expanding the forces and responses in the form of a Fourier series.

These terms may prove extremely cumbersome, on the other hand, when an attempt is made to deal with a problem of instability or transitory response. Fortunately the symmetrical properties of the rotor make it possible to eliminate these terms by a suitable change of variable.

This variable may be defined by the equations: /343

$$r_1(t) = \frac{1}{3}\sum_K s_K(t)$$

$$r_2(t) = \frac{2}{3}\sum_K \cos\theta_K(t)\, s_K(t)$$

$$r_3(t) = \frac{2}{3}\sum_K \sin\theta_K(t)\, s_K(t) \qquad (6.1)$$

with $\theta_K = \Omega t + \frac{2(K-1)\pi}{3}$

where r_1, r_2, r_3 are the new columns of generalized coordinates. These coordinates, which are defined by combining the coordinates for all three blades, constitute the rotor coordinates.

The inverse transformation may be written:

$$a_K(t) = r_1(t) + \cos\theta_K r_2(t) + \sin\theta_K r_3(t) \qquad (6.2)$$

$$\text{with } \theta_K = \Omega t + \frac{2(K-1)\pi}{3}.$$

Letting $r_2 = r_3 = 0$, it may be seen that $r_1(t)$ defines a type of vibration in which the deflection of all three blades is the same. This mode of vibration is termed a "collective mode."

Letting $r_1 = r_2 = 0$, it may be seen that $r_3(t)$ defines a type of vibration in which the deflection is antisymmetric in relation to the fixed reference plane $(\vec{i},\vec{k})$, related to the fuselage, since it is proportional to the sine of the azimuth (Fig. 1a).

Finally, letting $r_1 = r_3 = 0$, itmay be seen that $r_2(t)$ defines a type of vibration in which the deflection is antisymmetric in relation to the plane $(\vec{j}, \vec{k})$, since it is proportional to the cosine of the asimuth.

The vibration modes defined by the coordinates r_2 and r_3 are termed "cyclic modes."

Substituting Eq. (6.2) in Eqs. 5.1, 5.2 and 5.3 results in the following expressions:

$$2T = \dot{\theta}^2 I_{zT} + 6\dot{\theta}\Lambda\dot{r}_1 + 6\dot{\theta}^2\Gamma r_1 + 2\dot{\theta}\bar{q}A\dot{q} - \dot{\theta}^2\left[3\bar{r}_1\phi r_1 + \frac{3}{2}\bar{r}_2\phi r_2 + \frac{3}{2}\bar{r}_3\phi r_3\right] + \bar{q}M\ddot{q} +$$

$$+ 3\bar{r}_1\mu\dot{r}_1 + \frac{3}{2}\bar{r}_2\mu\dot{r}_2 + \frac{3}{2}\bar{r}_3\mu\dot{r}_3 + 3\dot{\theta}\left[\bar{r}_2\mu r_3 - \bar{r}_3\mu r_2\right] + \frac{3}{2}\dot{\theta}^2\left[\bar{r}_2\mu r_2 + \bar{r}_3\mu r_3\right] - \qquad (7.1)$$

$$- 2\dot{\theta}\left[3\bar{r}_1 H\dot{r}_1 + \frac{3}{2}\bar{r}_2 H\dot{r}_2 + \frac{3}{2}\bar{r}_3 H\dot{r}_3\right] + 2\bar{q}\left[3F\dot{r}_1 + \frac{3}{2}G\dot{r}_2 + \frac{3}{2}J\dot{r}_3\right] + 3\dot{\theta}\bar{q}\left[S - J\right]r_2 + 3\dot{\theta}\bar{q}\left[T + G\right]\dot{r}_3$$

$$2U = \bar{q}\,\Upsilon^{*}q + 3\bar{r}_1\Upsilon r_1 + \frac{3}{2}\bar{r}_2\Upsilon r_2 + \frac{3}{2}\bar{r}_3\Upsilon r_3 \qquad (7.2)$$

$$2D = \bar{\dot{q}}\beta^{*}\dot{q} + 3\bar{\dot{r}}_1\beta\dot{r}_1 + \frac{3}{2}\left[\bar{\dot{r}}_2\beta\dot{r}_2 + \bar{\dot{r}}_3\beta\dot{r}_3\right] + \frac{3}{2}\dot{\theta}^2\left[\bar{r}_2\beta r_2 + \bar{r}_3\beta r_3\right] + 3\dot{\theta}\left[\bar{\dot{r}}_2\beta r_3 - \bar{\dot{r}}_3\beta r_2\right]. \qquad (7.3)$$

II. 5. Movement Equations

The Lagrange equations relative to the generalized coordinates $\Delta\theta$, q and the functions r_i may be written:

$$\frac{d}{dt}\left(\frac{\partial T}{\partial\dot{\Delta\theta}}\right) - \frac{\partial T}{\partial\Delta\theta} + \frac{\partial U}{\partial\Delta\theta} + \frac{\partial D}{\partial\dot{\Delta\theta}} = \Phi_{\Delta\theta}$$

$$\frac{d}{dt}\left(\frac{\partial T}{\partial\dot{q}}\right) - \frac{\partial T}{\partial q} + \frac{\partial U}{\partial q} + \frac{\partial D}{\partial\dot{q}} = \Phi_q$$

$$\frac{d}{dt}\left(\frac{\partial T}{\partial\dot{r}_i}\right) - \frac{\partial T}{\partial r_i} + \frac{\partial U}{\partial r_i} + \frac{\partial D}{\partial\dot{r}_i} = \Phi_{r_i}\ i = 1, 2, 3$$

where the second members Φ represent the columns of generalized forces.

Replacing T, U and D by Eqs. (7.1), (7.2) and (7.3) respectively, one obtains the matrix equation:

$$m\ddot{Y} + B\dot{Y} + KY = \Phi \qquad (8)$$

where the column $Y = \begin{pmatrix} \Delta\theta \\ q \\ r_1 \\ r_2 \\ r_3 \end{pmatrix}$, and the matrices m, B, and K /344

are given by:

$m =$

I_{xT}		3Λ		
	M	$3F$	$\frac{3}{2}G$	$\frac{3}{2}J$
$3\bar{\Lambda}$	$3\bar{F}$	3μ		
	$\frac{3}{2}\bar{G}$		$\frac{3}{2}\mu$	
	$\frac{3}{2}\bar{J}$			$\frac{3}{2}\mu$

$\beta =$

		$6\Omega\Gamma$		
	$\beta^{\circ} + \Omega(A - \bar{A})$		$\frac{3}{2}\Omega(S - J)$	$\frac{3}{2}\Omega(T + G)$
$-6\Omega\bar{\Gamma}$		3β		
	$-\frac{3}{2}\Omega(\bar{S} - \bar{J})$		$\frac{3}{2}\beta$	$3\Omega\mu$
	$-\frac{3}{2}\Omega(\bar{T} + \bar{G})$		$-3\Omega\mu$	$\frac{3}{2}\beta$

$K =$

	γ°			
		$3(\gamma + \Omega^2\phi)$		
			$\frac{3}{2}[\gamma + \Omega^2(\phi - \mu)]$	$\frac{3}{2}\Omega\beta$
			$-\frac{3}{2}\Omega\beta$	$\frac{3}{2}[\gamma + \Omega^2(\phi - \mu)]$

II. 6. Natural Vibration Modes

Since a system of equations with constant coefficients have been obtained, the characteristic movements of the structure may easily be determined by considering the solutions for the system of equations without a second member.

Setting aside the dissipation forces (matrices β and β^*), which may be compensated by external forces, it is possible to define the characteristic vibration modes of the restraining structure, in the same way that these modes are defined for an aircraft design without rotating parts.

The characteristic solutions are in the form:

$$Y = Y' e^{i\omega t} \qquad (9)$$

where Y' is a complex vector and ω the characteristic rotative frequency.

Determination of the ω functions and the vectors Y' is reduced to a problem of characteristic values and characteristic vectors after substitution of Eq. (9) in Eq. (8) with no second member.

These solutions define natural vibrations in which the coordinates $\Delta\phi$, q, r_1, r_2 and r_3 are harmonic time functions at the rotative frequency ω.

If one considers the blade coordinates s_K, on the other hand, /345 which define the movement in relation to axes turning with the rotor, on the basis of Eq. (6.2) one obtains a combination of three sinusoidal vibrations with rotative frequencies of ω, $\omega + \Omega$ and $\omega - \Omega$.

Finally, it should be noted that when dissipation forces are not taken into account, matrix B possesses the antisymmetric property which characterizes gyroscopic coupling. In this case, the characteristic vectors Y' are known to be complex; this is manifested by relative phase shifts between the different variables, within the resultant vibration mode.

III. Experimental Check

The equations set up in the preceding section in order to determine the dynamic behavior of the fuselage-rotor assembly are based on rigorous theoretical development. Nevertheless there is some risk that the errors occurring in defining the dynamic characteristics of each substructure and in representing the connections between components may result in considerable error with regard to the dynamic characteristics of the entire assembly.

For this reason a series of tests and calculations was undertaken in order to check theory by experimentation.

Application of this theory to an actual helicopter at rest, which was treated in Ref. [4], had already yielded satisfactory results in 1971.

The check presented here was performed on a schematic helicopter model. The comparisons between theory and experiment deal with natural vibration modes of the rotor-fusilage assembly and their variations as a function of rotation speed. These modes have been determined experimentally by vibration tests, by analyzing the response to resonance frequencies.

III. 1 Experiment

Both the tests and the model will be described in another article.

At present the discussion will be limited to those details which must be known in order to interpret the comparisons of theory and experiment.

The "fuselage" of the model consisted of a rigid body connected to a frame by elastic straps (Fig. 2). The frame itself was supported by a flexible suspension system. The rotor, which consisted of three flexible bronze blades, was driven by an electric motor. The blades were inserted in the hub and were equipped with gauges for measurement of the bending stresses due to flapping and drag. The blades were locked at an incident angle of 0° and were not subject to spin (Ω = 0). The coning angle was also zero.

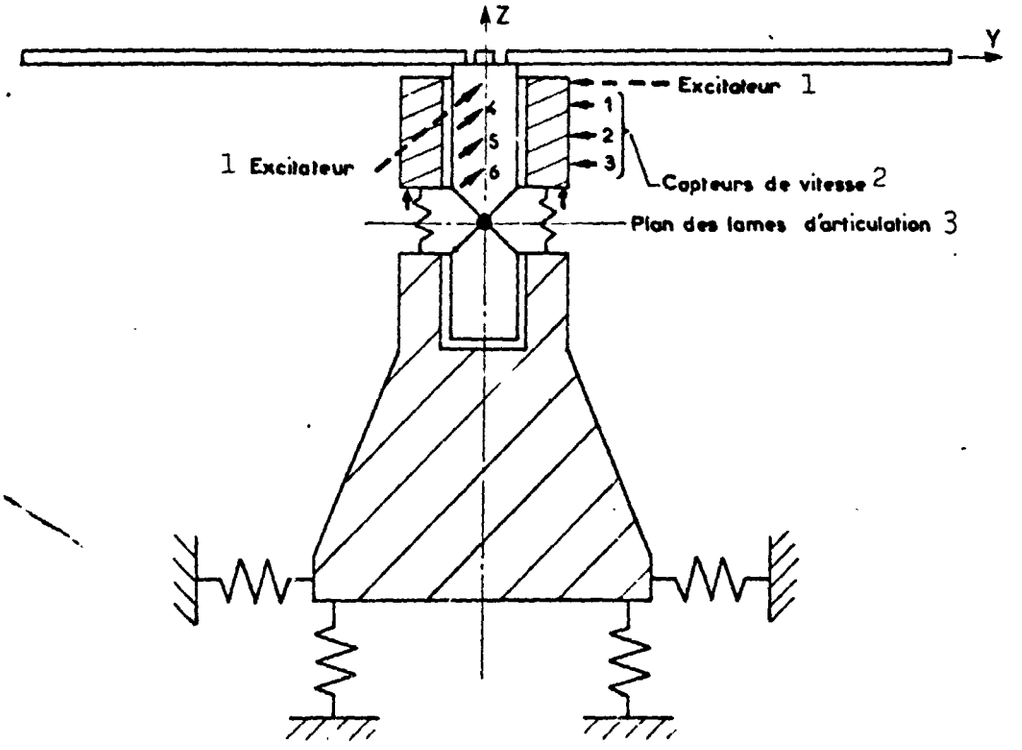

Fig. 2. Schematic diagram of model.

Key: 1. Exciter.
2. Speed sensors.
3. Plane of connecting straps.

The rotor being driven at a given rotation speed Ω, it was possible to excite the model by applying a known excitation force to the top of the fuselage. Since the damping of the structure was negligible, responses to the resonance frequencies virtually coincided with the characteristic vibration modes of the connected restraining system. The value of the resonance frequency and the spatial distribution of responses, defined to one affinity, were determined by means of the weight and stiffness distributions of the fuselage and blades, and the overall amplitude was determined by the damping of the structure.

For reasons of convenience, the measured responses were: /346

- the speed responses of the fuselage in the directions Ox and Oy, as a function of the altitude coordinate z (fig. 3a),
- the stress responses due to flapping and drag at several blade cross sections. Fig. 3b defines the cross sections equipped with flapping and drag gauges.

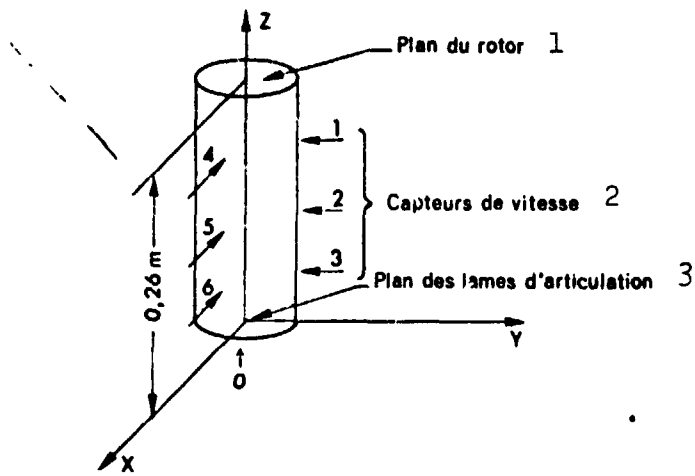

Fig. 3a Planes of measurement of speed responses of fuselage.

Key: 1. Plane of rotor.
2. Speed sensors.
3. Plane of connecting straps.

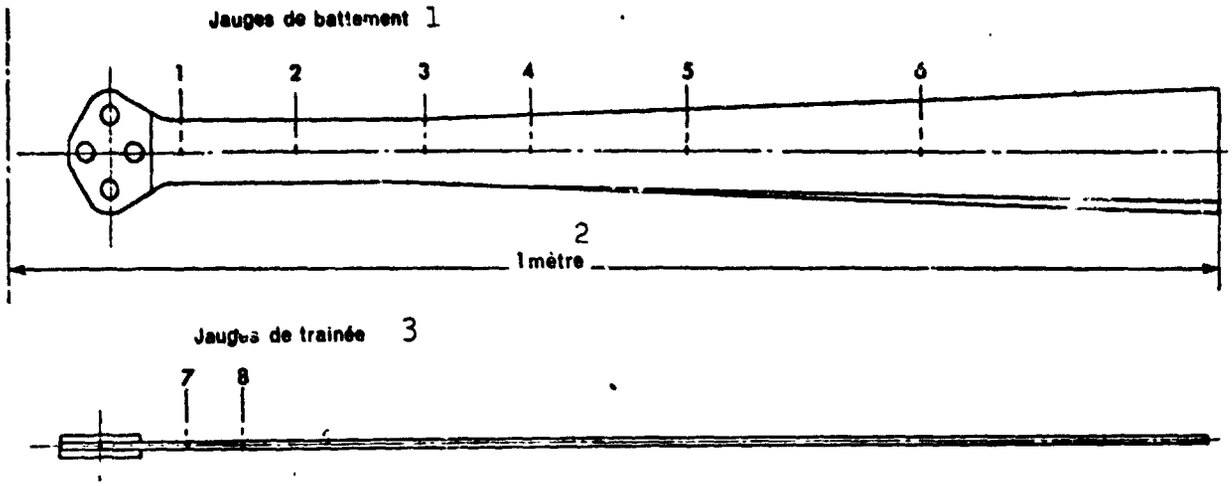

Fig. 3b. Distribution of stress measurement cross sections along blades.

Key: 1. Flapping gauges. 2. 1 meter. 3. Drag gauges.

The density of the blades and their stiffness were such that the aerodynamic forces generated by flapping and torsion vibrations were negligible in comparison to the inertial and elastic forces, and had no appreciable effect on the characteristic vibration modes.

Conventional vibration tests were initially performed on the different parts of the structure. The configurations tested included:

- the fuselage mounted on a frame, equipped with motor and hub but separate from blades,
- a blade inserted in a rigid support under the same conditions as it is inserted in the hub.

These tests furnished the characteristic branch modes which separately characterized the fuselage and the blades. Definition of these modes includes the characteristic fuselage and blade configurations defined in II.2 and the generalized magnitudes defined in II.3. that is, the generalized weights (diagonal matrices μ^* and μ) generalized stiffnesses (diagonal matrices γ^* and γ), and generalized viscosities (matrices β^* and β). Matrices β^* and β were assumed to be diagonal.

The distribution of speeds and the distribution of stresses in each normalized characteristic configuration were determined for the fuselage and for the blade, respectively.

III. 2. Calculations

The computational procedure used made it possible to determine the characteristic modes of the complete structure on the basis of the branch modes for the fuselage and the blades furnished by vibration tests.

Tables I and II indicate the frequency and nature of the modes considered in order to obtain the respective characteristics of the blades and the fuselage.

Table I /347

Characteristic mode for blade

Nature of mode	Frequency (Hz)
basic flapping	3.991
flapping, 1 knot	28.298
flapping, 2 knots	82 893
flapping, 3 knots	163.640
drag	32.289
torsion	79.983

Table II

Characteristic mode for fusilage

Nature of mode	Frequency (Hz)
roll	3.200
pitch	3.264
pumping	3.870
roll	10.596
pitch	10.936
roll	43.033
pumping	57.000
pitch	62.439

The vibration modes of the restraining system connected to the fuselage-rotor assembly are normally obtained with the use of Eqs. (8) by cancelling both the second member and matrices β^* and β and by solving the problem of characteristic values and characteristic vectors.

The latter factors make it possible to obtain spatial functions or "characteristic shapes" which define the spatial distribution of the various responses (movement response, speed, acceleration, stress response, etc.). Like the characteristic vectors, these shapes are determined to only one coefficient and must be normalized.

By comparing the modes computed in this way with the measured modes it is possible to assure that the stiffness and weight distribution is well represented in the calculations. However, it may also be to advantage to check to see that the dissipation forces are also well represented.

To make this check it is necessary to compute the response of the model to the excitation force applied during the test. For this purpose, the complete system of Eqs. (8) must be considered, introducing matrices β^* and β, as well as the second member, and the specific solution defining the response to harmonic excitation must be calculated. Since only excitation due to resonance is taken into account and since the structural damping is slight, a check may be made to determine whether the response effectively coincides with the characteristic mode; in this case, however, the overall amplitude depends on matrices β^* and β and is no longer indeterminate.

Whatever method is used, for each mode the calculations will yield the characteristic rotative frequency and a column vector which defines the generalized coordinates $\Delta\theta$, q, r_1, r_2 and r_3. The transformation formula (6.2) may be used to derive the blade coor-

dinates s_K. The rotor coordinat , r_1, r_2 and r_3 being harmonic time functions, with a rotative frequency ω, and θ_K being equal to $\Omega t + \frac{2\pi}{3}(K-1)$, it may be seen from Eq. (6.2) that s_K will be broken down into three sinusoid responses with rotative frequencies ω, $\omega + \Omega$, and $\omega - \Omega$.

The speed responses of the fuselage and the stress responses of the blades are determined by columns q and s_K, respectively, on the basis of the measured speed and stress values in the fuselage and blade branch modes.

In the same way as s_K, the stress response of the rotating blades consists of three rotative frequency components ω, $\omega + \Omega$ and $\omega - \Omega$. For the fuselage, on the other hand, the response is harmonic to rotative frequency ω.

When the structure vibrates in a natural mode of the connected restraining system, the spatial amplitude and phase distribution of the three components will be said to define the characteristic shape.

III.3. Results

The vibration tests and calculations for the fuselage-rotor assembly have been performed in two configurations:

-- an initial configuration in which the blades are in the same state as they are during the branch vibration test, and which may be termed the "clean blade configuration."

-- a second configuration obtained by adding an additional weight to the end of each blade equal to 18% of its own weight, and which may be termed the "loaded blade configuration."

Calculation of characteristic modes on the basis of characteristic values and characteristic vectors has been applied primarily to the clean blade configuration, and calculation of forced response to the loaded blade configuration.

It should be noted that branch vibration tests were not performed on loaded blades and that the influence of the additional weight was determined by calculation on the basis of the modes of the clean blades.

III. 3. 1. Clean Blade Configuration

Fig. 4 shows the theoretical and experimental variations in characteristic frequencies $f = \frac{\omega}{2\pi}$ as a function of rotation speed Ω. The markings on the graph approximately indicate the different modes.

There is excellent agreement between the theoretical and experimental frequencies. The sole exception is a slight deviation in the frequency of the "fuselage-cyclic drag" mode, which becomes attenuated as the rotation speed increases. This deviation is probably due to the static deflection of the blades under the effect of their own weight. This effect, which was not introduced into these calculations becomes negligible with centrifugal force.

In the course of their variations as a function of rotation speed, the frequency of the "fuselage-cyclic drag" and "second cyclic flapping" modes pass very close to each other, a phenomenon which may be attributed to a pseudo-increase for $\frac{\Omega}{2\pi} = 6.5$ Hz. An actual /348 increase would have been impossible due to the restraining coupling, which tends to separate the frequencies.

The points marked A, B, C and D on the graph indicate the modes and rotation speeds for which complete readings were obtained for the responses defining the characteristic shapes. A

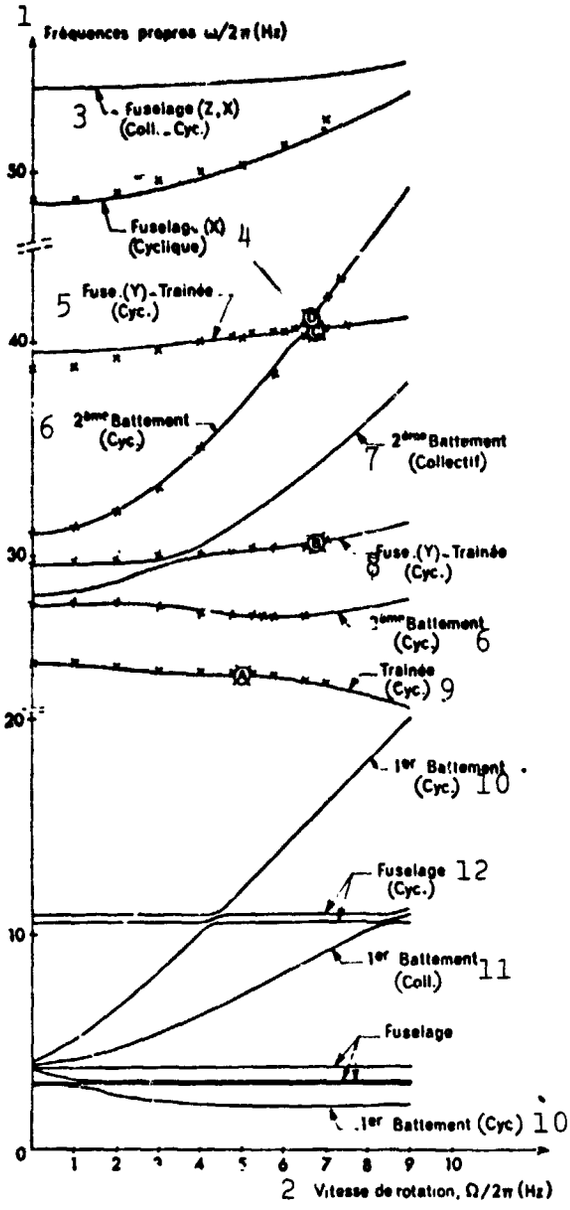

Fig. 4. Clean blade configuration. Variations in characteristic frequencies.
—— Calculated
x Experiment

Key: 1. Characteristic frequency; 2. Rotation speed; 3. Fuselage (Z,X) (cumulative-cyclic); 4. Fuselage (X) (cyclic); 5. Fuselage (Y)-drag (cyclic); 6. Second flapping (cyclic); 7. Second flapping (cumulative); 8. Fuselage (Y)-drag (cyclic); 9. Drag (cyclic); 10. First flapping (cyclic); 11. First flapping (cumulative); 12. Fuselage (cyclic).

comparison of the theoretical and experimental shapes is given in Fig. 5 for mode A, Fig. 6 for mode B, Fig. 7 for mode C, and Fig. 8 for mode D.

Due basically to experimental considerations, the comparison of theory and experiment was limited to the amplitudes, or moduli, of the different responses. The curves representing the development of these moduli as a function of the spatial coordinate sometimes possess cusps due to the passage of nodal points.

It should also be recalled that the theoretical shapes result from the calculation of characteristic vectors and are defined to only one coefficient. The theoretical shapes presented have thus been normalized to one measurement point and

/349

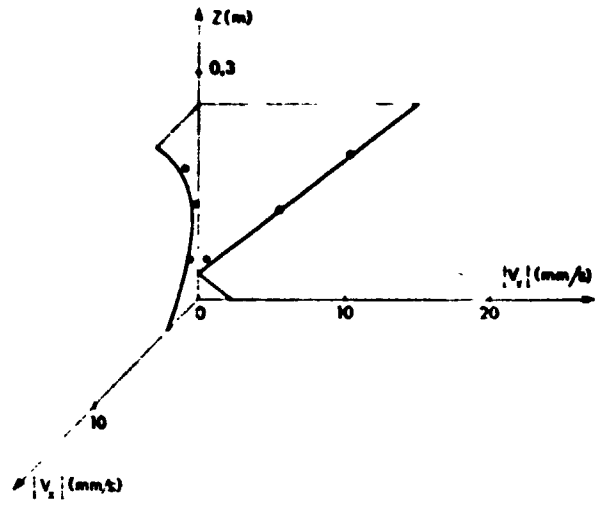

Fig. 5 a. Characteristic shape of mode A, clean blade configuration. Distribution of oscillation speed along the vertical axis of the fuselage.
—— Normalized theoretical characteristic shapes
o Experimental points
$\Omega/2\pi$ = 5.0 Hz. $\omega/2\pi$ = 24.4 Hz.

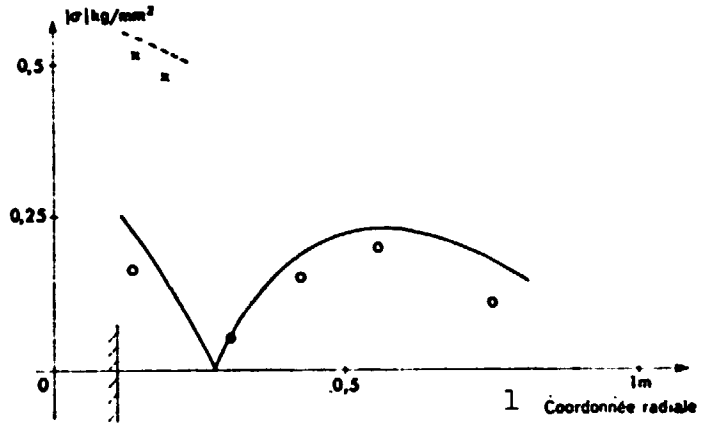

Fig. 5 b. Characteristic shape of mode A, clean blade configuration. Distribution of flapping and drag stresses along blades. Component $\Omega + \omega$.
—— Calculations } Stresses due to
o Experiment } flapping
--- Calculations } Stresses due to
x Experiment } drag
$\Omega/2\pi$ = 5.0 Hz. $\omega/2\pi$ = 24.4 Hz.

Key: 1. Radial coordinate

the comparison of theory and experiment makes it possible to estimate the similarity of relative responses, and especially, the ratio between the response of the blades and that of the fuselage, or between drag stresses and flapping stresses on the blade.

Fig. 5 a shows the distribution of oscillation speed components for the fuselage along the directions OX and OY as a function of the altitude coordinate z, in mode A.

Figs. 5 b and 5 c deal with blade drag and flapping stresses in a single mode and show the moduli as a function of the radial coordinate. Vibration at a rotative frequency $\omega + \Omega$ is a combination of drag and flapping (Fig. 5 b), while vibration at a rotative frequency $\omega - \Omega$ consists almost entirely of drag

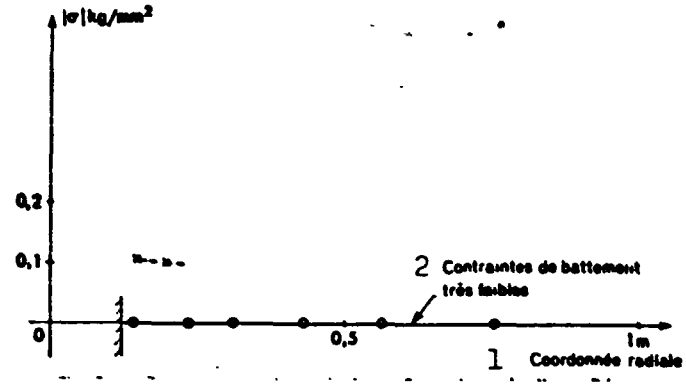

Fig. 5 c. Characteristic shape of mode A, clean blade configuration. Distribution of flapping and drag stresses along blades. Component ω - Ω.
—— Calculations } Stresses due to
o Experiment } flapping
--- Calculations } Stress due to
x Experiment } drag
Ω/2π = 5.0 Hz. ω/2π = 24.4 Hz.

Key: 1. Radial coordinate; 2. Very slight flapping stresses

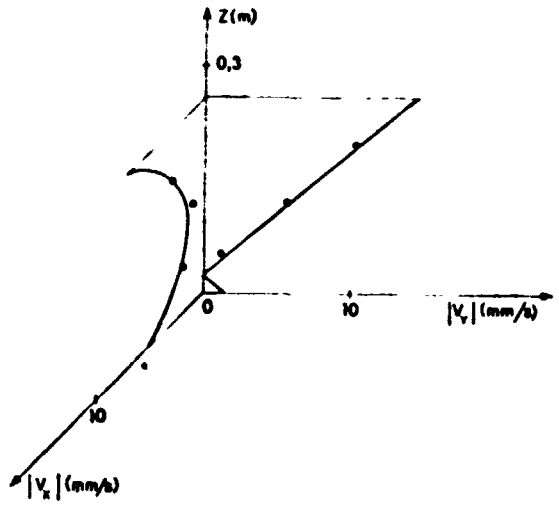

Fig. 6 a. Characteristic shape of mode B, clean blade configuration. Distribution of oscillation speed along vertical axis of fuselage.
—— Normalized theoretical characteristic shape
o Experimental points
Ω/2π = 6.66 Hz.
ω/2π = 30.37 Hz.

(Fig. 5 c). Vibration at rotative frequency ω is virtually negligible and has not been shown.

The characteristic theoretical and experimental shapes resulting from Fig. 5 a, 5 b and 5 c compare satisfactorily.

The above statements also apply to Figs. 6 a, 6 b and 6 c.

Figs. 7 and 8 pertain to the two modes C and D whose characteristic frequences are very close, as shown by Fig. 4. Despite this relative proximity, which may be the cause of experimental or theoretical difficulties, comparison of the relative responses is still fairly satisfactory. Nevertheless, a more significant deviation in stresses due to drag may be noted in the component at rotative frequency ω- Ω (Fig. 7 c).

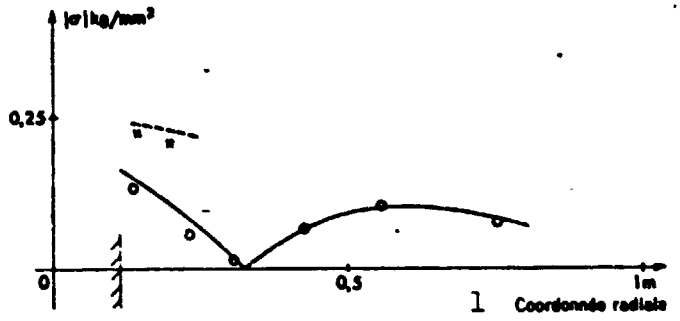

Fig. 6 b. Characteristic shape of mode B, clean blade configuration. Distribution of flapping and drag stresses along blades. Component $\omega + \Omega$.

—— Calculations } Stresses due
o Experiment } to flapping
--- Calculations } Stresses due
x Experiment } to drag

$\Omega/2\pi$ = 6.66 Hz
$\omega/2\pi$ = 30.37 Hz.

Key: 1. Radial coordinate

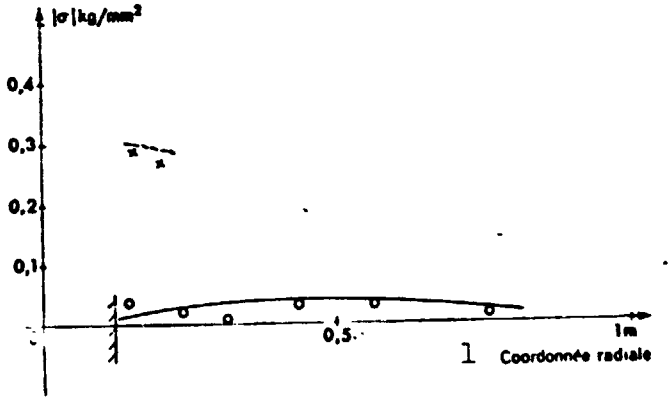

Fig. 6 c. Characteristic shape of mode B, clean blade configuration. Distribution of flapping and drag stresses along blades. Component $\omega - \Omega$.

—— Calculations } Stresses due
o Experiment } to flapping
---- Calculations } Stresses due
x Experiment } to drag

$\Omega/2\pi$ = 6.66 Hz
$\omega/2\pi$ = 30.37 Hz.

Key: 1. Radial coordinate

Analysis of the behavior of the characteristic shapes of these curves as a function of rotation speed shows that the proximity of the two characteristic frequencies within the zone of pseudo-increase where modes C and D are located (Fig. 4) is accompanied by rapid changes in the two characteristic shapes. These changes are illustrated by Fig. 9 and 10.

Fig. 9 shows, as a function of Ω, the variations in a speed response, a flapping stress and a drag stress observed in accordance with the mode designated as "second flapping" in Fig. 4. It may be noted that most of the parameters shown undergo sudden variations at a rotation speed in the neighborhood of $\Omega/2\pi$ = 6.5 Hz. /354

In an analogous manner, Fig. 10 shows variations in the mode termed "fuselage-drag" in Fig. 4. Once again,

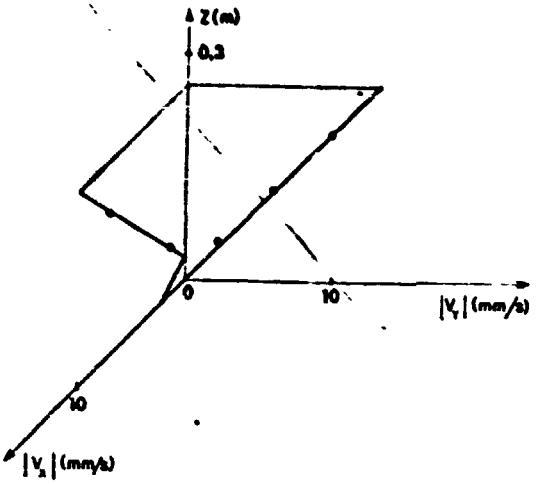

Fig. 7 a. Characteristic shape of mode C, clean blade configuration. Distribution of oscillation speed along the vertical axis of the fuselage.
—— Normalized theoretical characteristic shape
o Experimental points
$\Omega/2\pi$ = 6.66 Hz
$\omega/2\pi$ = 40.52 Hz

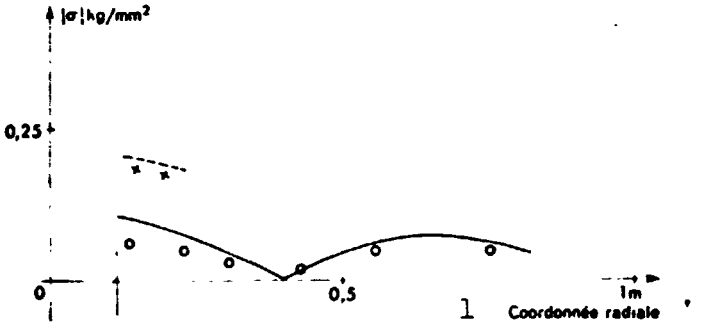

Fig. 7 b. Characteristic shape of mode C, clean blade configuration. Distribution of flapping and drag stresses on blades. Component $\omega + \Omega$.
—— Calculations } Stresses due to flapping
o Experiment }
--- Calculations } Stresses due to drag
x Experiment }
$\Omega/2\pi$ = 6.66 Hz
$\omega/2\pi$ = 40.52 Hz

Key: 1. Radial coordinate

an abrupt variation in the shape parameters may be noted in the vicinity of $\Omega/2\pi$ = = 6.5 Hz.

Despite this rapid change, which could result in extreme sensitivity to rotation speed in the vicinity of 6.5 Hz, it may be noted that the experimental points are favorably located in relation to the theoretical curves.

III.3.2. Loaded Blade Configuration

The theoretical and experimental variations in characteristic frequency for the loaded blade configuration are shown in Fig. 11. There is excellent agreement for most of the modes investigated. However, there is a slight deviation, which becomes attenuated with the rotation speed, in the frequency of the "fuselage-cyclic drag"

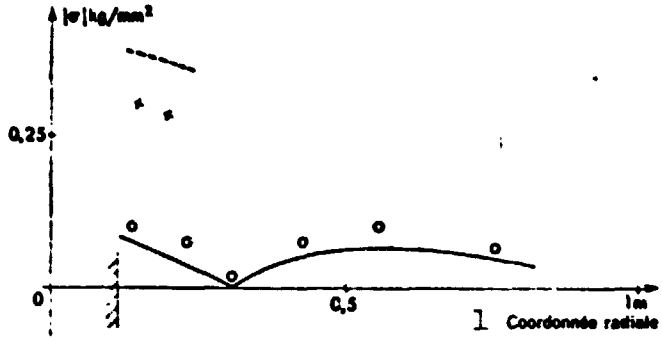

Fig. 7 c. Characteristic shape of mode C, clean blade configuration. Distribution of flapping and drag stresses on blades. Component $\omega - \Omega$.

—— Calculations } Stresses due
o Experiment } to flapping
--- Calculations } Stresses due
x Experiment } to drag

$\Omega/2\pi$ = 6.66 Hz
$\omega/2\pi$ = 40.52 Hz

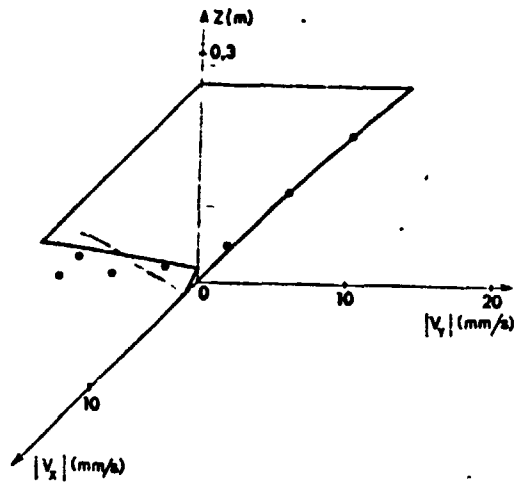

Fig. 8 a. Characteristic shape of mode D, clean blade configuration. Distribution of oscillation speed along vertical axis of fuselage.

—— Normalized theoretical characteristic shape
o Experimental points

$\Omega/2\pi$ = 6.66 Hz
$\omega/2\pi$ = 41.12 Hz.

mode. This deviation can probably be attributed to deflection of the blades under the effect of their own weight.

Complete measurements and calculations were performed for the modes defined by points E, F, G and H in the graph.

The experimental responses and normalized characteristic shapes are shown in Fig. 12 to 15, in the same way as for the clean blade configuration. Highly satisfactory agreement between the experimental and theoretical values may be noted.

However, as was mentioned at the beginning of Section III.3, calculations of forced response were performed for the loaded blade configuration, making it possible to predict the absolute value of the responses, taking the structural damping into account.

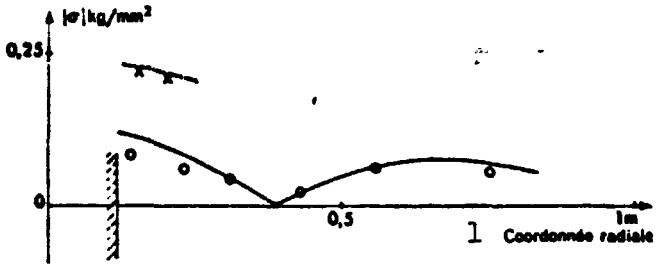

Fig. 8 b. Characteristic shape of mode D, clean blade configuration. Distribution of flapping and drag stresses on blades. Component $\omega + \Omega$.

—— Calculations } Stresses due to
o Experiment } flapping
--- Calculations } Stresses due to
x Experiment } drag

$\Omega/2\pi = 6.66$ Hz
$\omega/2\pi = 41.12$ Hz.

1. Radial coordinate

One point in this absolute response is given in Figs. 12 a, 13 a, 14 a and 15 a. Since it is known that the absolute response and the theoretical characteristic shape are related, this point serves to define the absolute response of the entire system and permits comparison with the experimental response. The absolute response may be noted to differ very little from the normalized shape and the experimental response for modes F, G and H (Figs. 13 a, 14 a and 15 a).

The deviation is much more marked for mode E (Fig. 12 a), which is basically a cyclic drag mode for the blades.

The presence of this deviation seems to indicate that the structural damping of the blades with respect to drag has been underestimated.

IV. Conclusion

The branch mode method treated in this article makes it possible to predict the dynamic characteristics of a helicopter structure. Theoretical analysis shows that the ideal restraining structure obtained without taking dissipation forces into account possesses relatively simple natural vibration modes due to the symmetry of the rotor.

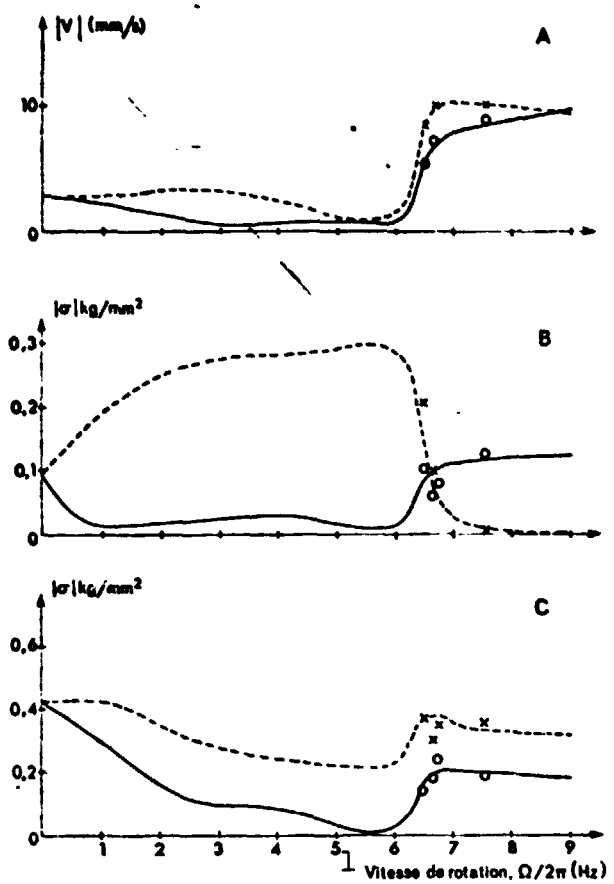

Fig. 9. Behavior of "second cyclic flapping" mode ($\omega/2\pi$ = 31.0 Hz at Ω = 0), as a function of $\Omega/2\pi$. Clean blade configuration.
A. Speed of fuselage, modulus (sensors 1 and 4)
—— Calculations } Direction X (4)
o Experiment }
--- Calculations } Direction Y (1)
x Experiment }
B. Flapping stress on blades, modulus (gauge 1).
—— Calculations } for $\omega + \Omega$
o Experiment }
--- Calculations } for $\omega - \Omega$
x Experiment }
C. Drag stress on blades, modulus (gauge 7).

Key: 1. Rotation speed

In calculation, the dynamic characteristics of the fuselage and the blades are defined separately by their characteristic modes. These modes may be determined experimentally by branch vibration tests, or they may be calculated using the finite elements method. The connection conditions between the blades and the hub and the inertial forces of coupling and rotation are introduced by the calculations.

The method was applied to a schematic helicopter model on which vibration tests were performed.

The branch modes characterizing the fuselage and the blades were determined experimentally.

A comparison of theoretical and experimental results has shown that the frequencies and

characteristic shapes for the curves, that is, the characteristics depending on inertia and stiffness distribution, were accurately predicted. On the other hand, the amplitude of responses to resonance, which depends on the structural damping, was not satisfactorily predicted in all cases.

The characteristic shapes were also found to be extremely sensitive to rotation speed within zones of pseudo-increase in frequency.

Finally, the characteristic frequency of the "fuselage-cyclic drag" mode appeared to be influenced by the static droop of the blades under their own weight, as long as the rotation speed was zero or slight.

Despite these problems, highly satisfactory results have been obtained. However, the fact should be taken into account that it was relatively simple to apply the theory to the model considered for the following reasons:

-- the structure was linear,
-- the hub was extremely rigid,
-- the connecting planes between the blades and hub were virtually nondeformable,
-- there was no coning angle for the rotor,
-- the blades were not subject to spin,
-- joints which might have introduced play or dry friction were avoided.

It is possible that application of this theory to a real helicopter would present problems which were not encountered here and which would necessitate additional precautions.

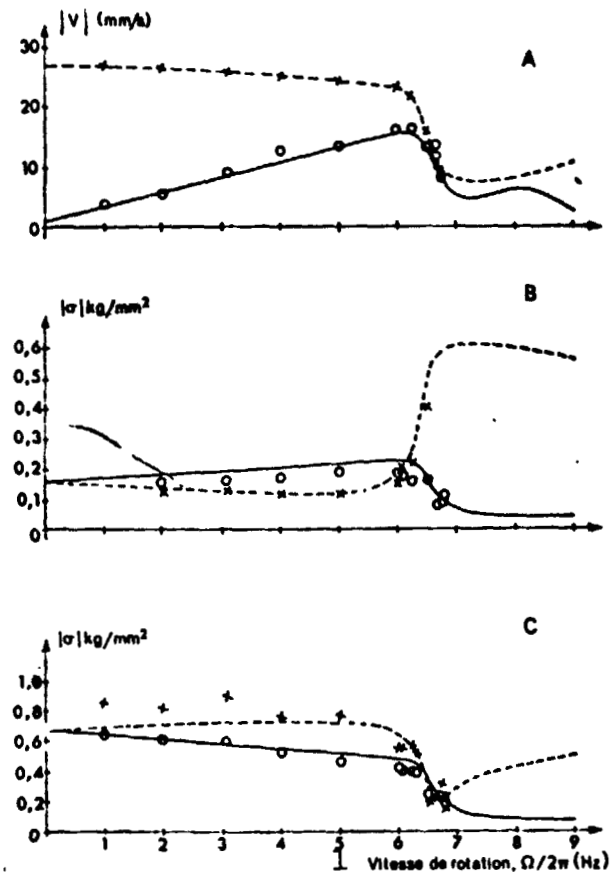

Fig. 10. Behavior of "fuselage (Y)-drag, cyclic" mode ($\omega/2\pi$ = 39.5 Hz at Ω = 0), as a function of $\Omega/2\pi$. Clean blade configuration

A. Speed of fuselage, modulus (sensors 1 and 4).

—— Calculations } Direction X (4)
o Experiment
--- Calculations } Direction Y (1)
x Experiment

B. Flapping stress on blades, modulus (gauge 1).

—— Calculations } for $\omega + \Omega$
o Experiment
--- Calculations } for $\omega - \Omega$
x Experiment

C. Drag stress on blades, modulus (gauge 7).

Key: 1. Rotation speed

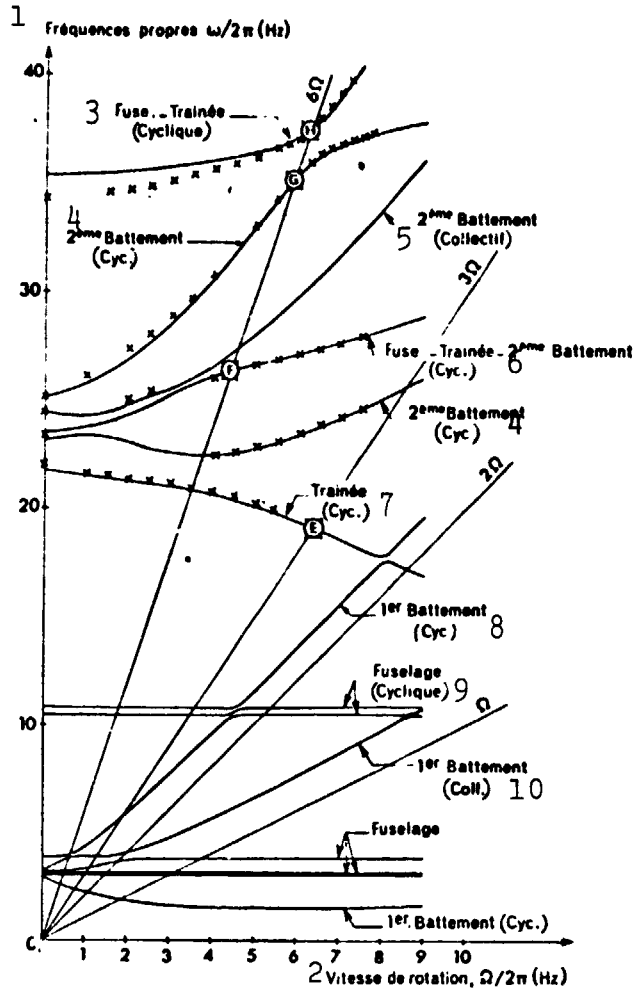

Fig. 11. Loaded blade configuration: variations in characteristic frequencies.
—— Calculations
x Experiment

Key: 1. Characteristic frequency
2. Rotation speed
3. Fuselage-drag (cyclic)
4. Second flapping (cyclic)
5. Second flapping (cumulative)
6. Fuselage-drag-second flapping (cyclic)
7. Drag (cyclic)
8. First flapping (cyclic)
9. Fuselage (cyclic)
10. First flapping (cumulative)

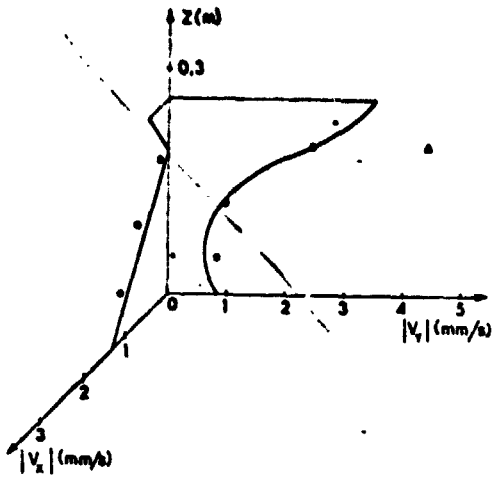

Fig. 12 a. Characteristic shape of mode E, loaded blade configuration. Distribution of oscillation speed along vertical axis of fuselage.
—— Normalized theoretical characteristic shape
▲ Computed response
o Experiment points (response to harmonic excitation).
$\Omega/2\pi$ = 6.35 Hz
$\omega = 3\Omega$.

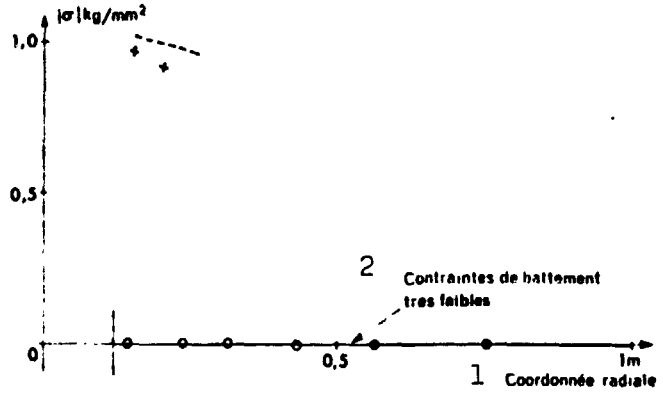

Fig. 12 b. Characteristic shape of mode E, loaded blade configuration. Distribution of flapping and drag stresses on blades. Component $\omega + \Omega$.
—— Calculations } Stresses due to flapping
o Experiment
--- Calculations } Stresses due to drag
x Experiment
$\Omega/2\pi$ = 6.35 Hz
$\omega = 3\Omega$.

Key: 1. Radial coordinate
2. Flapping stresses very slight

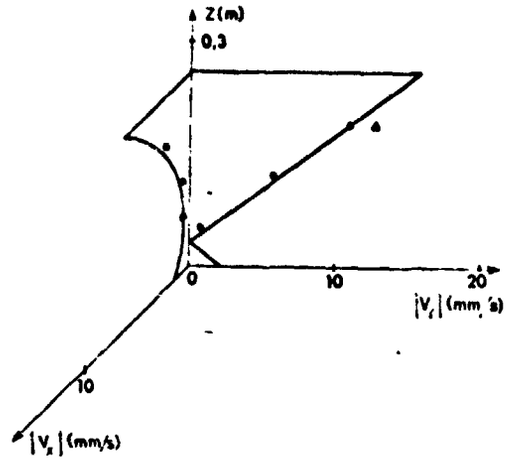

Fig. 13 b. Characteristic shape of mode F, loaded blade configuration. Distribution of oscillation speed along vertical axis of fuselage.
—— Normalized theoretical characteristic shape
▲ Computed response
o Experiment points (response to harmonic excitation)
$\Omega/2\pi$ = 4.37 Hz
$\omega = 6\Omega$.

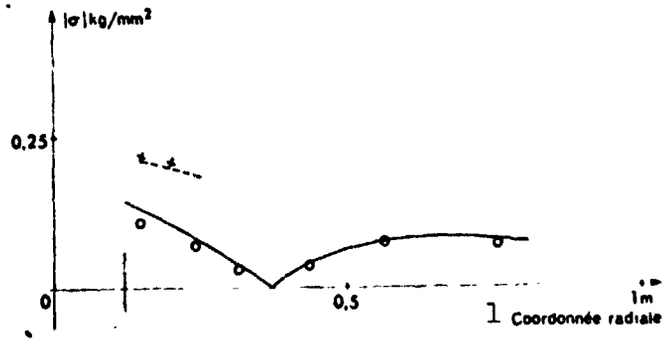

Fig. 13 b. Characteristic shape of mode F, loaded blade configuration. Distribution of flapping and drag stresses on blades. Component $\omega + \Omega$.
—— Calculations } Stresses due to flapping
o Experiment }
--- Calculations } Stresses due to drag
x Experiment }
$\Omega/2\pi$ = 4.37 Hz
$\omega = 6\Omega$.

Key: 1. Radial coordinate

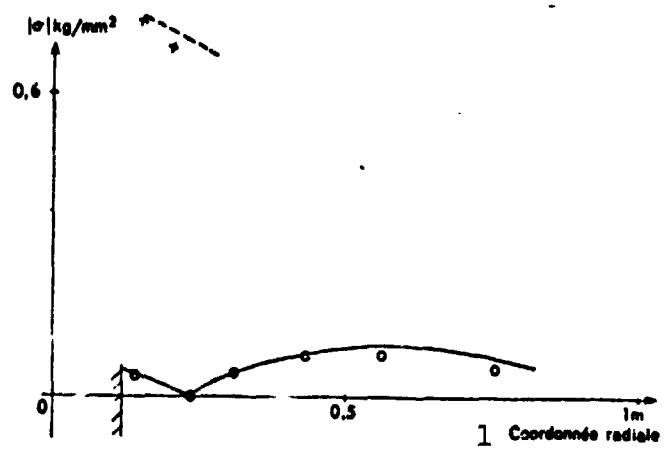

Fig. 13 c. Characteristic shape of mode F, loaded blade configuration. Distribution of flapping and drag stresses on blades. Component $\omega - \Omega$.

—— Calculations } Stresses due to flapping
o Experiment }
--- Calculations } Stresses due to drag
x Experiment }

$\Omega/2\pi = 4.37$ Hz
$\omega = 6\Omega$.

Key: 1. Radial coordinate

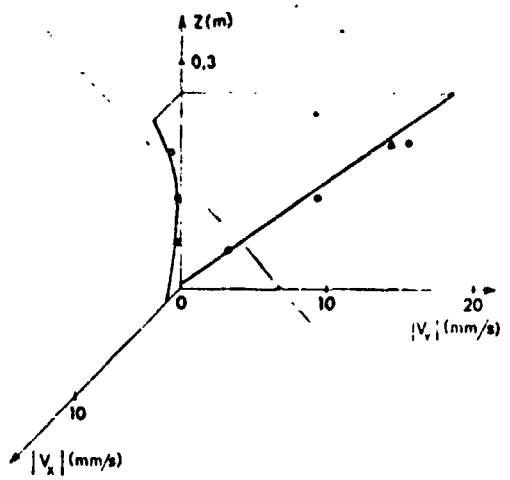

Fig. 14 a. Characteristic shape of mode G, loaded blade configuration. Distribution of oscillation speed along the vertical axis of fuselage.

—— Normalized theoretical characteristic shape
• Computed response
o Experiment points (response tc harmonic excitation).

$\Omega/2\pi = 5.8$ Hz
$\omega = 6\Omega$.

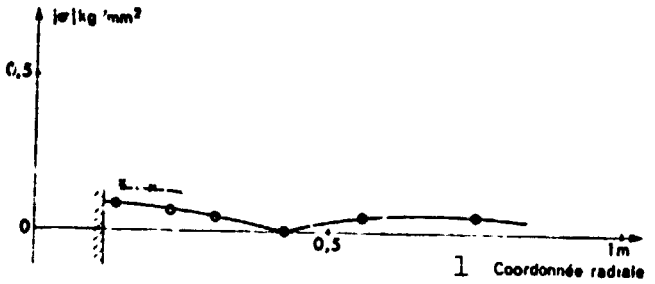

Fig. 14 b. Characteristic shape of mode G, loaded blade configuration. Distribution of flapping and drag stresses on blades. Component $\omega + \Omega$.

——Calculations } Stresses due to flapping
o Experiment
--- Calculations } Stresses due to drag
x Experiment

$\Omega/2\pi = 5.8$ Hz
$\omega = 6\Omega$.

Key: 1. Radial coordinate

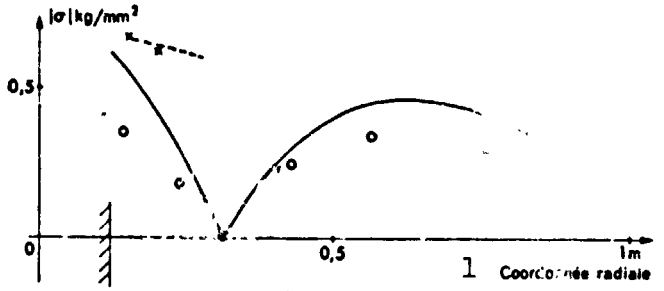

Fig. 14 c. Characteristic shape of mode G, loaded blade configuration. Distribution of flapping and drag stresses on blades. Component $\omega - \Omega$.

—— Calculations } Stresses due to flapping
o Experiment
--- Calculations } Stresses due to drag
x Experiment

$\Omega/2\pi = 5.8$ Hz
$\omega = 6\Omega$.

Key: 1. Radial coordinate

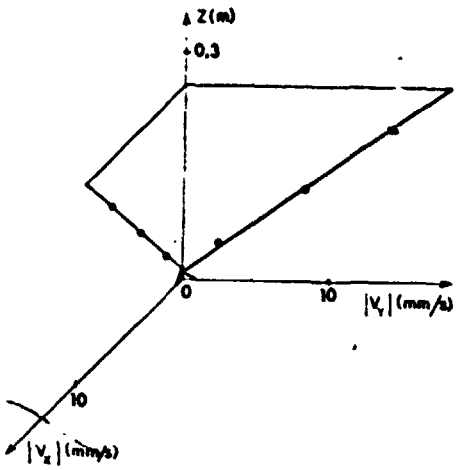

Fig. 15 a. Characteristic shape of mode H, loaded blade configuration. Distribution of oscillation speed along vertical axis of fuselage.
—— Normalized theoretical characteristic shape.
• Computed response
o Experimental points (response tc harmonic excitation).
$\Omega/2\pi$ = 6.2 Hz
$\omega = 6\Omega$.

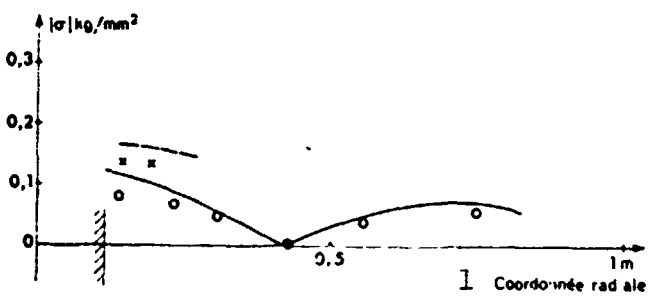

Fig. 15 b. Characteristic shape of mode H, loaded blade configuration. Distribution of flapping and drag stresses on blades. Component $\omega + \Omega$.
—— Calculations } Stresses due to flapping
o Experiment
--- Calculations } Stresses due to drag
x Experiment
$\Omega/2\pi$ = 6.2 Hz
$\omega = 6\Omega$.

Key: 1. Radial coordinate

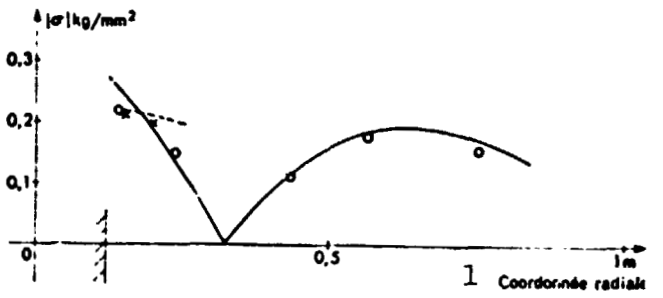

Fig. 15 c. Characteristic shape of mode H, loaded blade configuration. Distribution of flapping and drag stresses on blades. Component $\omega - \Omega$.

—— Calculations } Stresses due to flapping
o Experiment }

--- Calculations } Stresses due to drag
x Experiment }

$\Omega/2\pi = 6.2$ Hz

$\omega = 6\Omega$.

Key: 1. Radial coordinate

REFERENCES

1. Dat, R., "Representation of an airfoil line given vibrational movement by an acceleration dipole line," Rech. Aerosp., No. 133, 45 (Nov.-Dec. 1969).

2. Costes, J.J., "Calculation of non-stationary aerodynamic forces acting on the blades of a helicopter rotor," Rech. Aerosp. No. 2, 91 (1972).

3. Dat, R., "Airfoil theory applied to airscrews and helicopters," Rech. Aerosp. No. 4, 245 (1973).

4. Hutin, P.M., "Use of the branch mode method to predict the vibrational characteristics of helicopters in flight," Rech. Aerosp. No. 1, 41 (1971).

5. Dat, R., "Aeroelasticity of rotary wings," in Helicopter Aerodynamics and Dynamics, AGARD L.S. 63 (1973).